



ELSEVIER

Applied Mathematics and Computation 107 (2000) 1–26

APPLIED
MATHEMATICS
AND
COMPUTATION

www.elsevier.nl/locate/amc

On the behaviour of time discretisations of the electric field integral equation

Penny J. Davies^{a,1}, Dugald B. Duncan^{b,*}

^a *Department of Mathematics, University of Strathclyde, Glasgow, G1 1XH, UK*

^b *Department of Mathematics, Heriot-Watt University, Edinburgh, EH14 4AS, UK*

Abstract

We derive a separation of variables solution for time-domain electromagnetic scattering from a perfectly conducting infinite flat plate. The time dependent part of the equations are then used as a model problem in order to study the effects of various time discretisations on the full scattering problem. We examine and explain how exponential and polynomial instabilities arise in the approximation schemes, and show that the time averaging which is often used in an attempt to stabilise solutions of the full problem acts to destabilise some of the schemes. Our results show that two of the time discretisations can produce good results when coupled with a space-exact approximation, and indicate that they will be useful when coupled with an accurate enough spatial approximation. © 2000 Elsevier Science Inc. All rights reserved.

AMS: 65L20; 65R20; 78-08; 78A45

Keywords: Electromagnetic scattering; Numerical analysis; Time-domain; Retarded potential

1. Introduction

Finding the scattered field that results when a transient (non-harmonic) electric field is incident on a perfect conductor is an important problem in computational electromagnetics. One popular approach is to use a boundary integral formulation to compute the current and charge that are induced on the conductor's surface, since this is then sufficient to determine the scattered field

* Corresponding author. E-mail: d.b.duncan@ma.hw.ac.uk

¹ E-mail: penny.davies@strath.ac.uk

at any point in space (see e.g. Ref. [1]). This leads to a coupled system of differential and retarded potential integral equations (RPIEs) (so called because the time argument of the integrand is delayed) which then must be solved numerically. There seems to be agreement that it is better to approximate the system in a form that uses only first order derivatives in space and time than one which uses second order derivatives [2–4] and we use the first order formulation of the problem given by Rynne in Ref. [3].

We non-dimensionalise the equations by using units in which the permeability and permittivity (and hence the speed of light) are equal to 1. Suppose that the (known) electric field $\mathbf{E}(\mathbf{x}, t)$ is incident on the perfectly conducting surface \mathcal{P} . The surface current $\mathbf{J}(\mathbf{x}, t)$ and charge $\rho(\mathbf{x}, t)$ induced on \mathcal{P} satisfy the continuity equation

$$\frac{\partial \rho}{\partial t} + \text{Div } \mathbf{J} = 0, \quad (1)$$

(Div denotes the surface divergence), and the scalar (ϕ) and vector (\mathbf{A}) potentials are defined in terms of them by the RPIEs

$$\phi(\mathbf{x}', t) = \frac{1}{4\pi} \int_{\mathcal{P}} \frac{\rho(\mathbf{x}, t - R)}{R} dS \quad (2)$$

and

$$\mathbf{A}(\mathbf{x}', t) = \frac{1}{4\pi} \int_{\mathcal{P}} \frac{\mathbf{J}(\mathbf{x}, t - R)}{R} dS, \quad (3)$$

where $R = |\mathbf{x} - \mathbf{x}'|$. The potentials satisfy the electric field integral equation (EFIE)

$$\left(\frac{\partial \mathbf{A}}{\partial t} + \text{grad } \phi \right)_{\text{tan}} = \mathbf{E}_{\text{tan}}, \quad (4)$$

where the subscript “tan” denotes the tangential component of a quantity on the surface \mathcal{P} . As initial conditions all quantities are assumed to be zero for all times $t \leq 0$.

This integro-differential system is typically solved numerically by first expanding in terms of spatial basis functions and then approximating the resulting equations in time [2–6]. Unfortunately numerical approximations of systems involving RPIEs are often unstable, and result in exponentially growing oscillating errors in the solution (see e.g. Refs. [2,3,7]). Hence it is important to investigate the stability of numerical approximations of the system (1)–(4), so that the causes of instability can be determined and eliminated.

The full approximate system is extremely difficult to analyse because of the interaction between the integral and differential equations and the combined

effects of spatial and temporal approximations, but it is possible to deduce some useful stability results from Fourier analysis when \mathcal{P} is a large flat plate [8,9]. However, it can sometimes also be illuminating to analyse individual parts of the system separately. For example, the stability of numerical approximations of the scalar RPIE (2) has been considered in detail in Refs. [10,11]. In Ref. [11] a separation of variables approach (Fourier decomposition on an infinite flat plate) was used to analyse “space exact” time-stepping approximations of RPIEs (i.e., the spatial variation of solutions was treated exactly, allowing attention to be focussed on the time-stepping method).

It is known that averaging the computed solution in time is often effective in eliminating or reducing oscillating instabilities (see e.g. Refs. [2,6,10,12]). The type of averaging used must be chosen carefully however, since as shown in Ref. [11] the averaging strategy advocated by Vechinski and Rao in Ref. [6] actually destabilises the time-evolution of low spatial frequencies in approximate solutions of RPIEs when an accurate spatial representation of the solution is used. In contrast Rynne’s averaging procedure [2,12] eliminates high frequency instabilities without exciting low frequency modes.

Our aim here is to analyse time discretisations of the “space-exact” version of the full system (1)–(4) and we use a similar approach to that contained in Ref. [11] for a scalar RPIE. In particular we wish to analyse the interactions between time approximations of the differential and integral equations, both for basic (unaveraged) and time-averaged approximation schemes. The main motivation is that fully space and time discretised schemes are difficult to analyse, and we can gain useful insight into, and understanding of the full problem by examining this space-exact case.

Approximating the solution of the full scattering problem (1)–(4) is extremely computationally intensive. It takes $O(N^2)$ floating point operations to compute the current and charge at each time-step when there are N spatial basis functions. Solution algorithms therefore usually employ explicit schemes to approximate Eqs. (1) and (4), and low order methods for the RPIEs (2) and (3) based on piecewise linear interpolation in the time variation of the solution components [3,4,6]. For this reason we restrict our analysis to second order accurate (in time) schemes for the differential equations, and linear time interpolation (a second order approximation) for the integrals.

We begin by deriving the Fourier decomposed system and describing the time-stepping algorithms that we shall analyse (in Sections 2 and 3, respectively). We then carry out a stability analysis of the basic schemes in Section 4, explaining how exponential and polynomial instabilities can arise in the approximation schemes. Temporal averaging is often used in an attempt to stabilise solutions of the full problem, but it can act to destabilise some of the space-exact schemes as shown in Section 5. Numerical test results are used to indicate the accuracy of each scheme in Section 6, and we conclude with a discussion of our results.

2. Fourier decomposition

In this section we derive the system of ordinary differential equations (ODEs) and integral equations describing the evolution of a single spatial Fourier mode on an infinite flat conducting surface \mathcal{P} . This is analogous to the usual separation of variables technique for PDEs. For convenience we take \mathcal{P} to be the plane $x_3 = 0$.

The Fourier transform \hat{u} of a function $u(\mathbf{x})$ on \mathcal{P} is given by

$$\hat{u}(\boldsymbol{\omega}) \equiv \int_{\mathbb{R}^2} u(\mathbf{x}) e^{-i\mathbf{x}\cdot\boldsymbol{\omega}} d\mathbf{x}. \quad (5)$$

Taking the transform of the full scattering problem (1)–(4) yields the system of ODEs and Volterra integral equations

$$\dot{\sigma} + \boldsymbol{\omega} \cdot \mathbf{F} = 0, \quad (6)$$

$$\psi(t) = \int_0^t J_0(\omega R) \sigma(t-R) dR, \quad (7)$$

$$\dot{\mathbf{a}} - \boldsymbol{\omega} \psi = \mathbf{e}, \quad (8)$$

$$\mathbf{a}(t) = \int_0^t J_0(\omega R) \mathbf{F}(t-R) dR, \quad (9)$$

in terms of the Fourier frequency $\boldsymbol{\omega}$ (regarded as a parameter), where $\omega = |\boldsymbol{\omega}|$ and J_0 is the first kind Bessel function of order zero, and we have made the change of variables

$$\hat{\rho} = i\sigma, \quad \hat{\phi} = i\psi/2,$$

$$\hat{\mathbf{J}} = \mathbf{F}, \quad \hat{\mathbf{A}} = \mathbf{a}/2, \quad \text{and} \quad \hat{\mathbf{E}} = \mathbf{e}/2. \quad (10)$$

These are the equations we study in the rest of the paper.

Note that σ and \mathbf{F} can be eliminated by differentiating Eq. (7) with respect to time (using the initial condition that $\sigma(0) = 0$), substituting for $\dot{\sigma}$ from Eq. (6) and using Eq. (9) to replace the integral term, to yield another ODE

$$\dot{\psi} = -\boldsymbol{\omega} \cdot \mathbf{a}. \quad (11)$$

This equation in combination with Eq. (8) forms a self-contained system for ψ and \mathbf{a} . Similarly, differentiating Eq. (9) with respect to t using the initial condition that $\mathbf{F}(0) = \mathbf{0}$, we obtain

$$\dot{\mathbf{a}}(t) = \int_0^t J_0(\omega R) \dot{\mathbf{F}}(t-R) dR,$$

and hence it follows from Eq. (8) that,

$$\int_0^t J_0(\omega R) \left\{ \dot{\mathbf{F}}(t-R) - \omega\sigma(t-R) - \boldsymbol{\varepsilon}(t-R) \right\} dR = 0,$$

where we have defined $\boldsymbol{\varepsilon}(t)$ by

$$\boldsymbol{e}(t) = \int_0^t J_0(\omega R) \boldsymbol{\varepsilon}(t-R) dR \tag{12}$$

(assuming that $\boldsymbol{e}(0) = 0$). Thus we also obtain the ODE

$$\dot{\mathbf{F}} = \omega\sigma + \boldsymbol{\varepsilon} \tag{13}$$

which forms a self-contained system for σ and \mathbf{F} when combined with the continuity Eq. (6). Any consistent approximation scheme for the system (6)–(9) should also reduce to an approximation for Eqs. (11) and (13).

3. Time-stepping algorithms

In this section we describe four different numerical approximations of the transformed system (6)–(9). Each of these schemes can be regarded as a time discretised but space-exact approximation of the full scattering problem (1)–(4) on an infinite flat plate, since the original problem can be recovered by taking the inverse Fourier transform and using the change of variables Eq. (10). The schemes all use the trapezoidal rule to approximate the integrals in Eqs. (7) and (9), since this corresponds to the usual approximation made for the full numerical system (see e.g. Refs. [3–6]), in which the integrand is linearly interpolated in time between successive solution components.

The first scheme corresponds to the solution algorithm used by Rynne [3] to solve the semi-discrete system of equations that results from Eqs. (1)–(4) once the current and charge have been approximated in space by finite element basis functions. It consists of a mixture of explicit and implicit approximations for the individual equations (6)–(9). When the approximations are used in the correct order each solution component is updated without the need to solve algebraic equations – in other words the scheme is semi-implicit. Scheme 2 uses a different approximation for the ODE (8), but is otherwise the same as Scheme 1.

The third scheme looks similar to the first two, but in this case the approximations are based on a fully staggered grid with σ and ψ approximated at times offset by $\Delta t/2$ from those used for the \mathbf{F} and \mathbf{a} approximations. The use of a staggered grid is a common approach to solving systems of hyperbolic PDEs [13], Ch. 4.8 and given that the underlying system is Maxwell’s equations, this seems a sensible avenue to explore. The final scheme uses the

trapezoidal rule for the integrals and ODE approximations, and hence is fully implicit. It is included here mainly for comparison with the others (the trapezoidal ODE approximation is stable for all values of the time-step), since an implicit numerical scheme of this type would be complicated (although not too costly) to implement in practice.

Once the schemes have been defined we show that they contain approximations of the ODEs (11) and (13), since this proves useful in the stability analysis carried out in Section 4.

3.1. Scheme definitions

The time-step used for the discretisation is taken to be Δt and we use the short-hand notation that $u^n = u(t^n) = u(n \Delta t)$ for any function $u(t)$. We also set $\mathbf{v} = \Delta t \boldsymbol{\omega}$ and $J_0^m = J_0(m\mathbf{v})$. The initial value terms are explicitly included in the scheme definitions, but recall that we are assuming that all quantities are zero for time $t \leq 0$.

Scheme 1: Rynne's scheme [3] for Eqs. (1)–(4) corresponds to using the following central difference approximations for Eqs. (6) and (8)

$$\sigma^n = \sigma^{n-2} - 2\mathbf{v} \cdot \mathbf{F}^{n-1}, \quad (14)$$

$$\mathbf{a}^n = \mathbf{a}^{n-2} + \frac{\mathbf{v}}{2}(\psi^n + 2\psi^{n-1} + \psi^{n-2}) + \frac{\Delta t}{2}(\mathbf{e}^n + 2\mathbf{e}^{n-1} + \mathbf{e}^{n-2}), \quad (15)$$

for $n \geq 1$. The two retarded potential integrals (7) and (9) are approximated by the trapezoidal rule (corresponding to linear interpolation in time), giving

$$\psi^n = \Delta t \left\{ \sigma^n / 2 + \sum_{m=1}^{n-1} J_0^m \sigma^{n-m} + J_0^n \sigma^0 / 2 \right\}, \quad (16)$$

$$\mathbf{a}^n = \Delta t \left\{ \mathbf{F}^n / 2 + \sum_{m=1}^{n-1} J_0^m \mathbf{F}^{n-m} + J_0^n \mathbf{F}^0 / 2 \right\}, \quad (17)$$

for $n \geq 1$. Scheme 1 consists of the four equations (14)–(17) solved in the order given above for σ^n , \mathbf{a}^n , ψ^n and then \mathbf{F}^n , after rearranging Eq. (17).

Scheme 2: The second scheme we consider uses Eqs. (14), (16) and (17) from Scheme 1, but the approximation of the EFIE equation (8) is replaced by

$$\mathbf{a}^n = \mathbf{a}^{n-2} + 2\mathbf{v}\psi^{n-1} + 2 \Delta t \mathbf{e}^{n-1}. \quad (18)$$

This has the same leap-frog (central difference approximation) structure as Eq. (14).

Scheme 3: This scheme uses “staggered” time levels for different components: \mathbf{F} and \mathbf{a} are needed at integer multiples of Δt , and σ and ψ at integer plus

one half multiples of Δt . The two differential equations (6) and (8) are approximated by a leap-frog formula with step Δt , giving

$$\sigma^{n-1/2} = \sigma^{n-3/2} - \mathbf{v} \cdot \mathbf{F}^{n-1}, \tag{19}$$

$$\mathbf{a}^n = \mathbf{a}^{n-1} + \mathbf{v}\psi^{n-1/2} + \Delta t e^{n-1/2}, \tag{20}$$

for $n \geq 1$. The scalar potential integral (2) is approximated by linear interpolation between integer plus one half multiples of Δt

$$\psi^{n-1/2} = \Delta t \left\{ \sigma^{n-1/2}/2 + \sum_{m=1}^{n-1} J_0^m \sigma^{n-1/2-m} + J_0^0 \sigma^{-1/2}/2 \right\}, \tag{21}$$

and the trapezoidal rule approximation (17) is again used for the integral equation (3).

Scheme 4: This scheme uses the trapezoidal rule for both the ODEs and integral equations, and hence is fully implicit. The differential equations (6) and (8) are approximated by

$$\sigma^n = \sigma^{n-1} - \frac{\mathbf{v}}{2} \cdot (\mathbf{F}^n + \mathbf{F}^{n-1}) \tag{22a}$$

and

$$\mathbf{a}^n = \mathbf{a}^{n-1} + \frac{\mathbf{v}}{2}(\psi^n + \psi^{n-1}) + \frac{\Delta t}{2}(e^n + e^{n-1}) \tag{22b}$$

for $n \geq 1$. The trapezoidal rule approximations (16) and (17) are used for the retarded potential integral equations (2) and (3).

3.2. Approximation of the ODEs for ψ and \mathbf{a}

Here we investigate how the four schemes described above approximate the property that Eqs. (6), (7) and (9) can be reduced to the ODE (11) when the zero initial conditions are used. We shall derive the ODE approximation for Eq. (11) that results from Scheme 1, and just state the approximations obtained from the other three schemes.

Recall that Eq. (11) was obtained by differentiating Eq. (7) in time, substituting for $\dot{\sigma}$ and then using Eq. (9) to replace the integral term. The corresponding operations for the Scheme 1 approximations are to difference (16) in time, substitute for the differenced σ terms from Eq. (14), and then use Eq. (17) to replace the integral summation.

Central differencing Eq. (16) with step $2 \Delta t$ about t^{n-1} gives

$$\psi^n - \psi^{n-2} = \Delta t \left\{ (\sigma^n - \sigma^{n-2})/2 + \sum_{m=1}^{n-2} J_0^m (\sigma^{n-m} - \sigma^{n-2-m}) + J_0^{n-1} \sigma^1 \right\},$$

where we have used $\sigma^0 = 0$. Substituting for the σ central differences from Eq. (14) yields

$$\psi^n - \psi^{n-2} = -2 \Delta t \mathbf{v} \cdot \left\{ \mathbf{F}^{n-1} / 2 + \sum_{m=1}^{n-2} J_0^m \mathbf{F}^{n-1-m} \right\} + \Delta t J_0^{n-1} \sigma^1,$$

then using Eq. (17) and the fact that $\sigma^1 \equiv 0$ by Eq. (14) and the assumption that all quantities are zero for $t \leq 0$ we get the standard leap-frog approximation of Eq. (17), i.e.

$$\text{Scheme 1:} \quad \psi^n = \psi^{n-2} - 2\mathbf{v} \cdot \mathbf{a}^{n-1} \quad (23)$$

Using a similar argument it can be shown that the other three schemes reduce to the following approximations for Eq. (11):

$$\text{Scheme 2:} \quad \psi^n = \psi^{n-2} - 2\mathbf{v} \cdot \mathbf{a}^{n-1}, \quad (24)$$

$$\text{Scheme 3:} \quad \psi^{n-1/2} = \psi^{n-3/2} - \mathbf{v} \cdot \mathbf{a}^{n-1}, \quad (25)$$

$$\text{Scheme 4:} \quad \psi^n = \psi^{n-1} - \frac{\mathbf{v}}{2} \cdot (\mathbf{a}^n + \mathbf{a}^{n-1}). \quad (26)$$

The *Scheme 2* approximation of the two ODEs (8) and (11) is a pair of leap-frog formulae. The approximate solution splits into two disjoint solution sets generated with $n = 0, 2, 4, \dots$ and $n = 1, 3, 5, \dots$. These are $\{\psi^{\text{ev}}, \mathbf{a}^{\text{od}}\}$ and $\{\psi^{\text{od}}, \mathbf{a}^{\text{ev}}\}$ where “ev” stands for even integers and “od” for odd. *Scheme 3* gives the same leap-frog scheme as *Scheme 2* (with n odd there), but the time-step size is halved here. This scheme is designed to explicitly select only one of the disjoint solution sets which appears in *Scheme 2*. The ODE pair (8) and (11) is approximated by the trapezoidal rule for *Scheme 4*.

3.3. Approximation of the ODEs for σ and \mathbf{F}

We now investigate how the ODE (13) derived from Eqs. (7)–(9) is approximated by the schemes. Again we only derive the *Scheme 1* approximation for Eq. (13) and state the others.

Starting with Eq. (15) from *Scheme 1*, we substitute for \mathbf{a}^n and \mathbf{a}^{n-2} from Eq. (17) and $\psi^{n-2}, \psi^{n-1}, \psi^n$ from Eq. (16) to obtain (after rearrangement and division by Δt)

$$\mathbf{E}^n / 2 + \sum_{m=1}^{n-1} J_0^m \mathbf{E}^{n-m} = 0$$

for $n \geq 1$, where

$$\mathbf{E}^k \equiv \mathbf{F}^k - \mathbf{F}^{k-2} - \frac{\mathbf{v}}{2} (\sigma^k + 2\sigma^{k-1} + \sigma^{k-2}) - \frac{1}{2} (\mathbf{e}^k + 2\mathbf{e}^{k-1} + \mathbf{e}^{k-2})$$

for all $k \geq 1$ and all quantities are zero for $k \leq 0$. The vector sequence $\{\mathbf{e}^n: n = 0, 1, \dots\}$ is defined by the following trapezoidal rule approximation of the RPIE (12):

$$\mathbf{e}^0 = 0, \quad \Delta t \left\{ \mathbf{e}^n / 2 + \sum_{m=1}^{n-1} J_0^m \mathbf{e}^{n-m} \right\} = \mathbf{e}^n \tag{27}$$

for $n \geq 1$. It is easy to show that $\mathbf{E}^k = \mathbf{0}$ for all $k \geq 0$, and so Scheme 1 reduces to the following approximation of Eq. (13):

$$\text{Scheme 1:} \quad \mathbf{F}^n = \mathbf{F}^{n-2} + \frac{\mathbf{v}}{2} (\sigma^n + 2\sigma^{n-1} + \sigma^{n-2}) + \frac{\Delta t}{2} (\mathbf{e}^n + 2\mathbf{e}^{n-1} + \mathbf{e}^{n-2}) \tag{28}$$

for $n \geq 1$.

Using a similar argument it can be shown that the other three schemes reduce to the following approximations for Eq. (13):

$$\text{Scheme 2:} \quad \mathbf{F}^n = \mathbf{F}^{n-2} + 2\mathbf{v}\sigma^{n-1} + 2 \Delta t \mathbf{e}^{n-1}, \tag{29}$$

$$\text{Scheme 3:} \quad \mathbf{F}^n = \mathbf{F}^{n-1} + \mathbf{v}\sigma^{n-1/2} + \Delta t \mathbf{e}^{n-1/2}, \tag{30}$$

$$\text{Scheme 4:} \quad \mathbf{F}^n = \mathbf{F}^{n-1} + \frac{\mathbf{v}}{2} (\sigma^n + \sigma^{n-1}) + \frac{\Delta t}{2} (\mathbf{e}^n + \mathbf{e}^{n-1}), \tag{31}$$

with $\mathbf{e}^{n-1/2}$ defined by

$$\mathbf{e}^{1/2} = 0, \quad \Delta t \left\{ \mathbf{e}^{n-1/2} / 2 + \sum_{m=1}^{n-1} J_0^m \mathbf{e}^{n-1/2-m} \right\} = \mathbf{e}^{n-1/2}. \tag{32}$$

As for Eq. (11), Schemes 2 and 3 result in leap-frog approximations for Eq. (13), and Scheme 4 gives the trapezoidal rule.

4. Stability of the basic schemes

We now examine the stability of the four schemes described in Section 3 for the integro-differential system (6)–(9). We begin by writing each approximation as a vector difference equation and use amplification matrices to characterise its stability. This is analogous to the stability analysis carried out for a scalar RPIE in Refs. [10,11], and for the fully discretised (i.e. space and time approximated) scheme in Refs. [8,9]. This approach allows the stability properties of each scheme to be investigated and compared numerically for different values of the scaled frequency $\mathbf{v} = \omega \Delta t$, and the results of this are summarised in Fig. 1.

However more insight into the schemes' behaviour (for this unaveraged system) can be obtained by considering their alternative formulation as

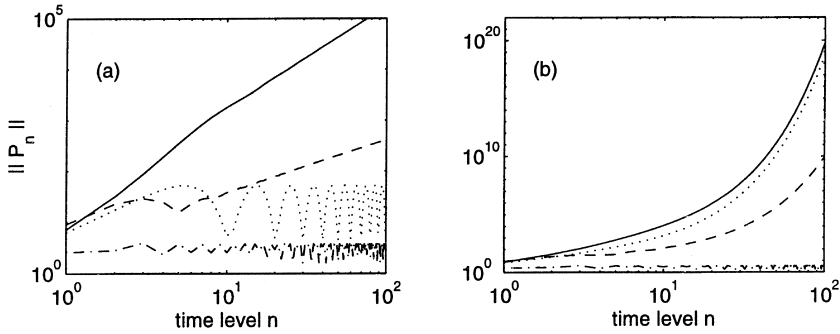


Fig. 1. Graphs of the amplification matrices $\|P^n\|_2$ against time level n for $v = \Delta t(1, 2)$ with Δt adjusted so that v is (a) 5% below and (b) 2% above the predicted stability limit for Schemes 1 (solid), 2 (dashed) and 3 (dotted). Scheme 4 (dash-dot) is unconditionally stable, and Δt is set equal to the maximum of that used for the other schemes.

approximations of the ODE pairs (8) and (11) for (σ, \mathbf{a}) and Eqs. (6) and (13) for (ψ, \mathbf{F}) coupled by the RPIE (12). It has been shown in Ref. [11] that the trapezoidal rule gives stable solutions of RPIEs like Eq. (12), and in Section 4.2 we show that the stability limit for the approximations of each of the ODE pairs is the same as that computed by the respective amplification matrices in Section 4.1. The reasons for this and the causes of weak (i.e. polynomial) instabilities are discussed in Section 4.3.

4.1. Stability of the integro-differential system

Here we investigate the stability of Schemes 1–4 for the full integro-differential system (6)–(9). We examine how a perturbation of the approximate solution is propagated by the schemes. This is in the spirit of the definition of absolute stability given by Baker [14], Def. 6.1.

We begin by introducing the solution 6-vector

$$z^n = \begin{pmatrix} \sigma^n \\ \mathbf{F}^n \\ \psi^n \\ \mathbf{a}^n \end{pmatrix} \text{ for Schemes 1, 2, 3, } \quad z^n = \begin{pmatrix} \sigma^{n-1/2} \\ \mathbf{F}^n \\ \psi^{n-1/2} \\ \mathbf{a}^n \end{pmatrix} \text{ for Scheme 4}$$

and rewrite each of the schemes in the form

$$Q^0 z^n = \mathbf{b}^n + \frac{1}{2} Q^n z^0 + \sum_{m=1}^{n-1} Q^m z^{n-m} \quad \text{for } n \geq 1,$$

where we use the convention $\sum_{m=1}^0 \cdot \equiv 0$. The vector $\mathbf{b}^n \in \mathbb{R}^6$ contains the inhomogeneous terms from Eq. (8) and the $Q^m \in \mathbb{R}^{6 \times 6}$ are coefficient matrices determined by the particular form of the scheme. The problem has initial data $\mathbf{z}^n = \mathbf{0}$ for $n \leq 0$.

For Scheme 1 the matrices Q^m are derived from the algorithm defined by Eqs. (14)–(17) and are:

$$Q^0 = \begin{pmatrix} 1 & \cdot & \cdot & \cdot & \cdot & \cdot \\ \cdot & 1 & \cdot & \cdot & 2/\Delta t & \cdot \\ \cdot & \cdot & 1 & \cdot & \cdot & 2/\Delta t \\ -\Delta t/2 & \cdot & \cdot & 1 & \cdot & \cdot \\ \cdot & \cdot & \cdot & -v_1/2 & 1 & \cdot \\ \cdot & \cdot & \cdot & -v_2/2 & \cdot & 1 \end{pmatrix},$$

$$Q^1 = \begin{pmatrix} \cdot & -2v_1 & -2v_2 & \cdot & \cdot & \cdot \\ \cdot & -2J_0^1 & \cdot & \cdot & \cdot & \cdot \\ \cdot & \cdot & -2J_0^1 & \cdot & \cdot & \cdot \\ \Delta t J_0^1 & \cdot & \cdot & \cdot & \cdot & \cdot \\ \cdot & \cdot & \cdot & -v_1 & \cdot & \cdot \\ \cdot & \cdot & \cdot & -v_2 & \cdot & \cdot \end{pmatrix},$$

$$Q^2 = \begin{pmatrix} 1 & \cdot & \cdot & \cdot & \cdot & \cdot \\ \cdot & -2J_0^2 & \cdot & \cdot & \cdot & \cdot \\ \cdot & \cdot & -2J_0^2 & \cdot & \cdot & \cdot \\ \Delta t J_0^2 & \cdot & \cdot & \cdot & \cdot & \cdot \\ \cdot & \cdot & \cdot & v_1/2 & 1 & \cdot \\ \cdot & \cdot & \cdot & v_2/2 & \cdot & 1 \end{pmatrix},$$

$$Q^m = \begin{pmatrix} \cdot & \cdot & \cdot & \cdot & \cdot & \cdot \\ \cdot & -2J_0^m & \cdot & \cdot & \cdot & \cdot \\ \cdot & \cdot & -2J_0^m & \cdot & \cdot & \cdot \\ \Delta t J_0^m & \cdot & \cdot & \cdot & \cdot & \cdot \\ \cdot & \cdot & \cdot & \cdot & \cdot & \cdot \\ \cdot & \cdot & \cdot & \cdot & \cdot & \cdot \end{pmatrix}$$

for $m > 2$. The dots indicate a zero entry. The other schemes give rise to similar coefficient matrices.

The stability analysis involves investigating the evolution of a perturbation η^0 of an approximate solution sequence $\{\mathbf{z}^n: n = 0, 1, \dots\}$ introduced at the p th

step (where $p \geq 2$) and then followed through the subsequent time levels of the approximation. The perturbed solution sequence is $\{\mathbf{z}^0, \dots, \mathbf{z}^{p-1}, \mathbf{z}^p + \boldsymbol{\eta}^0, \mathbf{z}^{p+1} + \boldsymbol{\eta}^1, \dots\}$, and it is easy to show that the perturbations $\boldsymbol{\eta}^n$ satisfy

$$\mathcal{Q}^0 \boldsymbol{\eta}^n = \sum_{m=1}^n \mathcal{Q}^m \boldsymbol{\eta}^{n-m},$$

where the matrices \mathcal{Q}^m are as defined above. Essentially the same system is obtained for perturbations in the approximate solution sequence at levels $p = 0$ and $p = 1$.

We say that the scheme to generate the approximate solution is *stable* on the time interval $[0, T]$ if there is a constant C independent of Δt and n such that

$$\|\boldsymbol{\eta}^n\| \leq C \|\boldsymbol{\eta}^0\|$$

whenever $t^n \leq T$. This is equivalent to the standard Richtmyer and Morton definition [15], Section 4.6. The scheme is said to be *exponentially unstable* if there are constants $\lambda > 1$ and C such that at least one perturbation sequence satisfies

$$\|\boldsymbol{\eta}^n\| \geq C \lambda^n,$$

and *weakly unstable* otherwise (i.e. $\|\boldsymbol{\eta}^n\|$ can grow like a polynomial in n).

It can be shown (see e.g. Refs. [9,10] for more details) that the perturbations $\boldsymbol{\eta}^n$ for $n \geq 1$ introduced by perturbation $\boldsymbol{\eta}^0$ at time level $p \geq 2$ can be written as

$$\boldsymbol{\eta}^n = P^n \boldsymbol{\eta}^0,$$

where the P^n are 6×6 amplification matrices whose entries depend on the coefficient matrices \mathcal{Q}^m through the recursive formula

$$\mathcal{Q}^0 P^n = \sum_{m=1}^n \mathcal{Q}^m P^{n-m}$$

for $n \geq 1$ where $P^0 = I_6$, the 6×6 identity matrix. Clearly the scheme is stable if the matrix 2-norm of the P^n satisfies $\|P^n\|_2 \leq C$ for all $n \leq T/\Delta t$.

The stability of the four schemes is examined by evaluating $\|P^n\|_2$ for the respective amplification matrices at various values of \mathbf{v} . Schemes 1 and 3 appear to be exponentially unstable if $\mathbf{v} > 2$, and Scheme 2 to be exponentially unstable if $\mathbf{v} > 1$. Scheme 4 seems to be unconditionally stable (i.e. stable for all \mathbf{v}). These stability limits are confirmed by the ODE analysis in the next section. Fig. 1 shows typical graphs of $\|P^n\|_2$ against n for the four schemes with $\mathbf{v} = \Delta t(1, 2)$ where Δt is adjusted so that in the left plot \mathbf{v} is 5% under and in the right plot 20% over the predicted stability limit for each scheme. It is clear that above the stability limit the amplification matrices for Schemes 1–3 grow exponentially, while below the limit (after a short settling in period) Scheme 1 has $\|P^n\|_2 = O(n^2)$, Scheme 2 has $\|P^n\|_2 = O(n)$ and Scheme 3 has $\|P^n\|_2 = O(1)$. Scheme 4 satisfies $\|P^n\|_2 = O(1)$ in all cases.

4.2. Exponential instability of the ODE pair approximations

The stability analysis of the previous section can be used to predict whether a scheme for the system (6)–(9) will be stable or not at any particular value of \mathbf{v} . However it does not give much insight as to what causes the stability restrictions on \mathbf{v} , and this can be seen more clearly by considering the equivalent but reformulated set of equations consisting of the ODE pairs (8) and (11) for (σ, \mathbf{a}) and Eqs. (6) and (13) for (ψ, \mathbf{F}) linked together by the RPIE (12).

Regarding \mathbf{e} as the (known) forcing term and $\mathbf{z} = (\sigma, \mathbf{a}, \psi, \mathbf{F}, \boldsymbol{\varepsilon})^T \in \mathbb{R}^8$ as the (unknown) solution vector, we see that the system decouples into an ODE pair for the first three solution components and a coupled ODE–RPIE system for the last five. Thus necessary and sufficient conditions for exponential instability of a numerical approximation of the system are that either the approximation of the ODE pair (8) and (11) is exponentially unstable, or that the approximation of the remaining ODE–RPIE system is exponentially unstable. It has been shown in Ref. [11] that the trapezoidal rule approximations Eqs. (27) and (32) of the RPIE (12) are stable, and so the approximate solution $\boldsymbol{\varepsilon}$ will be bounded if \mathbf{e} is smooth. If \mathbf{e} is bounded but not smooth, e.g. $\mathbf{e}^n = (-1)^n \mathbf{e}$, then $\boldsymbol{\varepsilon}$ can grow like n . So provided \mathbf{e} is bounded, ψ^n and \mathbf{F}^n are the solutions of a pair of discretised ODEs whose right-hand side can grow at most like $O(n)$, and hence they cannot grow exponentially unless the approximation used for the homogeneous ODEs is exponentially unstable. Thus the complete system will be exponentially unstable if and only if either of the homogeneous ODE pair approximations are exponentially unstable.

This means that the numerical approximation will be at most weakly unstable if \mathbf{v} is within the stability limit for the ODEs, and we now carry out a stability analysis of the ODE schemes (Sections 3.2 and 3.3) with no forcing terms (i.e. take $\mathbf{e}, \boldsymbol{\varepsilon} \equiv \mathbf{0}$). The analysis is standard (see e.g. Ref. [16]) and we shall give brief details for Scheme 1 and just quote the stability limit for the other three schemes. We note that the ODE pair approximations have the same form for the \mathbf{a}, ψ and \mathbf{F}, σ equations, and so we need only consider one of them.

Note that this is a similar situation to that occurring in the “flat plate” EFIE algorithm used in Ref. [2] to compute only the induced current (and not the charge) when \mathcal{P} is a flat plate. The space-exact version of this is the system of equations (8), (11) and (9), and this algorithm is also at worst weakly unstable if neither of the approximations used for the ODE pair and individual RPIE are exponentially unstable [7].

When $\mathbf{e} \equiv \mathbf{0}$ the reduced version of Scheme 1 is

$$\begin{aligned} \psi^n &= \psi^{n-2} - 2\mathbf{v} \cdot \mathbf{a}^{n-1}, \\ \mathbf{a}^n &= \mathbf{a}^{n-2} + (\mathbf{v}/2)(\psi^n + 2\psi^{n-1} + \psi^{n-2}). \end{aligned} \tag{33}$$

The scheme is exponentially unstable if there is a solution of Eq. (33) of the form $(\psi^n, \mathbf{a}^n) = \lambda^n \mathbf{C}$ for some $\lambda \in \mathbb{C}$ with $|\lambda| > 1$ where \mathbf{C} is a non-zero, complex three-vector. Substituting this ansatz into Eq. (33) and dividing by λ^{n-2} gives

$$\mathcal{M}(\lambda)\mathbf{C} = \mathbf{0},$$

where $\mathcal{M}(\lambda)$ is the matrix

$$\begin{pmatrix} \lambda^2 - 1 & 2\lambda v_1 & 2\lambda v_2 \\ -(\lambda + 1)^2 v_1 / 2 & \lambda^2 - 1 & 0 \\ -(\lambda + 1)^2 v_2 / 2 & 0 & \lambda^2 - 1 \end{pmatrix}.$$

Hence the scheme is exponentially unstable if there is a value of λ with $|\lambda| > 1$ that satisfies $\det \mathcal{M}(\lambda) = 0$. The determinant of \mathcal{M} is zero if and only if $\lambda = \pm 1$ or

$$\lambda^2 + (v^2 - 2)\lambda + 1 = 0$$

for $v = |\mathbf{v}|$. The product of the roots of this quadratic is 1, and so necessary and sufficient conditions to rule out exponential instability are that both roots are equal to 1 in modulus. This can only happen if the roots are a complex conjugate pair, that is if $v \leq 2$. Thus Scheme 1 will be exponentially unstable when $v > 2$.

The stability limit for Scheme 3 is also $v \leq 2$, and that for Scheme 2 is $v \leq 1$. The trapezoidal rule Scheme 4 is unconditionally stable.

Note that this analysis indicates the relative stability of the four schemes when an accurate spatial representation is used for the full spatially dependent system. However, the stability properties of the full spatially dependent case depends in a rather complicated way on both the time-stepping and spatial approximations used, as well as the interaction between them. This is explored in detail in Refs. [8,9] for one algorithm using a mixed finite element on an equilateral spatial mesh.

4.3. Weak instability

As shown in Fig. 1, Schemes 1 and 2 admit weakly unstable solutions even when v is small enough to rule out exponential instability. We see below that these unstable solutions are oscillatory and solve the homogeneous ($\mathbf{e}^n \equiv 0$) versions of the difference equations approximating the ODE pairs for ψ, \mathbf{a} and σ, \mathbf{F} but do not satisfy the initial conditions that all quantities are zero for $t \leq 0$. However they can be excited by sharp changes in the incident field or possibly by rounding errors. Schemes 3 and 4 do not have oscillatory weak instabilities.

In Scheme 1, the ODE approximation (33) for (ψ, \mathbf{a}) in the homogeneous case $\mathbf{e}^n \equiv 0$ admits an oscillatory solution

$$\mathbf{a}^n = C(-1)^n \frac{\mathbf{v}}{v} + D(-1)^n \frac{\mathbf{v}_\perp}{v_\perp}, \quad \psi^n = C(n - n_0)(-1)^n v, \tag{34}$$

where \mathbf{v}_\perp is perpendicular to \mathbf{v} , and C, D, n_0 are arbitrary constants. The constants C, D are determined by the exact form and time of the “kick” that activates this solution, and of course linear combinations of such solutions are possible. The net effect is that $|\psi^n|$ can grow like $O(n)$.

This spurious solution also appears for the homogeneous (σ, \mathbf{F}) ODE pair, since this uses the same approximation. However the solution (34) also excites a different unstable mode in (σ, \mathbf{F}) , linked through the RPIE approximations (16) and (17). This does not have a simple closed form expression, but the growth of the instabilities can be investigated by examining the solution of the RPIE problem

$$(\Delta t/2)(J_0^0 u^n + J_0^n u^0) + \Delta t \sum_{m=1}^{n-1} J_0^{n-m} u^m = g^n \tag{35}$$

with forcing term g^n set equal to the spurious solution ψ^n or \mathbf{a}^n from Eq. (34), so that u^n behaves like σ^n or \mathbf{F}^n , respectively. This then shows that σ^n grows like n^2 and \mathbf{F}^n grows like n as n increases. Fig. 2 plots results with $v = 1$ and forcing term (a) $g^n = (-1)^n$ and (b) $g^n = (-1)^n (n - 10)$ (with $g^n = 0$ for $n \leq 10$) and the linear and quadratic growth of the solution with n is clear. Similar results are obtained for $0 \leq v \leq 2$.

Scheme 2 admits an oscillating solution in its ODE pairs which has the form for (ψ, \mathbf{a}) :

$$\mathbf{a}^n = D(-1)^n \frac{\mathbf{v}_\perp}{v_\perp}, \quad \psi^n = 0.$$

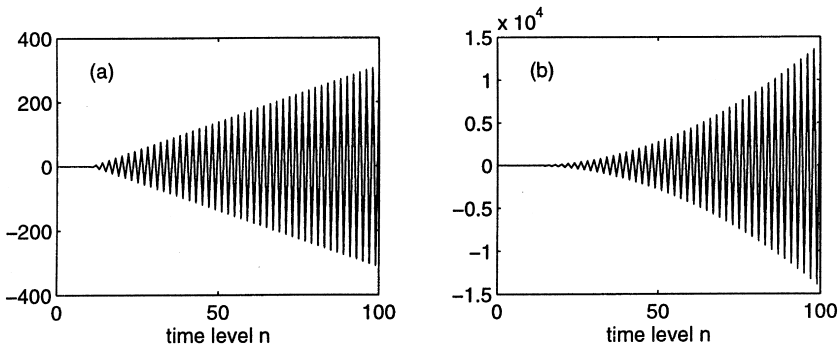


Fig. 2. Graphs of the solution of the discreted RPIE problem (35) with $v = 1$ and forcing term $e^n = 0$ for $n \leq 10$ and then (a) $e^n = (-1)^n$ and (b) $e^n = (-1)^n (n - 10)$.

This solution is possible because of the leap-frog form of the approximation. The F values generated through the RPIE approximation (17) then grow linearly in n as indicated by the numerical experiments.

One mechanism for exciting these spurious solutions is that a local event in the incident field e kicks the (ψ, a) ODE pair spurious solution into life and, because of its oscillatory nature, this is amplified through the RPIE approximations to give growing values of F and σ . An equivalent way of looking at it is that the local event in the incident field e translates into a long-term effect on the inhomogeneous term ε in the (σ, F) ODE pair approximations (28) and (29) and this in turn generates the polynomial growth in the (σ, F) approximations.

Fortunately these polynomial instabilities are excited very little by rounding error, but they may be excited by sharp changes in the incident field e . To test this and the general sensitivity of the schemes to the incident field data, we apply the schemes to a standard problem whose incident field consists of a single spike and is zero everywhere else – an approximate delta function. The result is shown in the first plot of Fig. 3 where we have used $v = [0.1, 0]$, $\Delta t = 0.1$ and a spike in the incident field at $n = 10$ given by $e^{10} = [1, 1]$. Note that this spike contains equal contributions in the v and v_{\perp} directions. We see, as predicted, that Scheme 2 has $\sigma^n = O(n)$ and Schemes 3 and 4 show no growth. However, the $O(n^2)$ growth of σ predicted for Scheme 1 does not appear.

To understand why Scheme 1 is more stable than expected, we modify the way the incident field appears through the ODE approximation by replacing Eq. (15) by

$$a^n = a^{n-2} + \frac{v}{2}(\psi^n + 2\psi^{n-1} + \psi^{n-2}) + 2 \Delta t e^{n-1} \tag{36}$$

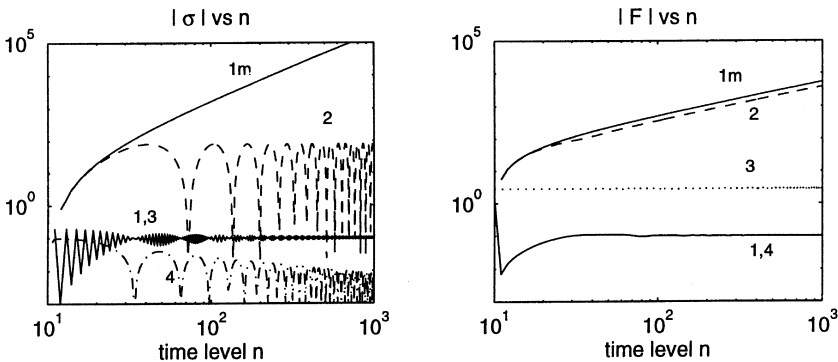


Fig. 3. Results of the standard “spike” test described in Section 4.3, with $v = (0.1, 0)$, $\Delta t = 0.01$. Scheme 1 (solid), 2 (dashed), 3 (dotted) and 4 (dash-dot) are indicated, as well the modified version of Scheme 1 (solid, marked “1m”) described by Eq. (36).

and perform the same spike test. We see in Fig. 3 that the modified Scheme 1 (marked “1m”) produces solutions that grow as expected. The reason for this is that the $(\frac{1}{4}, \frac{1}{2}, \frac{1}{4})$ averaging used on the incident field of Eq. (15) in Scheme 1 exactly cancels the polynomial instabilities.

4.4. Summary of stability results

The trapezoidal rule ODE approximation of Scheme 4 is unconditionally stable and the staggered grid leap-frog scheme used in 3 is stable subject to the reasonable step size restriction $\nu \leq 2$. Schemes 1 and 2 are exponentially unstable when $\nu > 2$ and $\nu > 1$ respectively, and are weakly unstable otherwise. This weak instability is observed in the growth of the amplification matrices described in Section 4.1 and explained in terms of a weak instability in the ODE pair approximations described above. However, this instability, if present in the full, space-dependent problem, would not grow quickly enough to cause serious problems since the massive amount of computer time required probably precludes running the problem for long enough to see it.

5. Time averaging

Although the trapezoidal rule is a stable approximation for space exact RPIEs like Eq. (9) [11], fully space and time discretised RPIE schemes are often extremely unstable, with exponentially oscillating instabilities [10]. For this reason a time averaging step is often added to solution algorithms for the full integro-differential system (1)–(4) to improve their stability (see e.g. Refs. [2,3,6,7,12]). A study of the scalar RPIE problem in Ref. [11] found that the time averaging formula (37) used by Rynne [12] produces more stable results than other methods, and we just consider this formula here.

Rynne’s averaging procedure is described in Ref. [3] (see also Refs. [2,8,9,12]) for the full system (1)–(4). One way to apply the averaging once the approximate solution is found up to time level t^{n-1} , is to take two further steps to compute the solution components at times t^n and t^{n+1} and then replace \mathbf{F}^n by

$$\frac{1}{4}\{\mathbf{F}^{n+1} + 2\mathbf{F}^n + \mathbf{F}^{n-1}\}. \quad (37)$$

All the components at time t^{n+1} are then deleted. On the face of it, this process takes two temporary steps forward to advance the approximate solution by only one step, and so is roughly twice as costly as the unaveraged scheme. However, after some rearrangement, this averaging can be done for only marginal extra cost to the basic algorithm (see e.g. Ref. [11]).

Restricting our attention to the Fourier transformed equations (6)–(9) we now describe Rynne's time averaging strategy for Scheme 1 of Section 3. Assuming that all the solution components $\{\sigma^m, \psi^m, \mathbf{a}^m; m \leq n-1\}$, $\{\mathbf{F}^m; m \leq n-2\}$ as well as the auxiliary quantity $\mathbf{F}^{n-1,*}$ have been computed, the next step is to update the solution to get $\sigma^n, \psi^n, \mathbf{a}^n, \mathbf{F}^{n-1}$ and $\mathbf{F}^{n,*}$. The algorithm is:

$$\begin{aligned}\sigma^{n,*} &= \sigma^{n-2} - 2\mathbf{v} \cdot \mathbf{F}^{n-1,*}, \\ \psi^{n,*} &= \Delta t \left(\sigma^{n,*}/2 + \sum_{m=1}^{n-1} J_0^m \sigma^{n-m} + J_0^n \sigma^0/2 \right), \\ \mathbf{a}^{n,*} &= \mathbf{a}^{n-2} + \frac{\mathbf{v}}{2} (\psi^{n,*} + 2\psi^{n-1} + \psi^{n-2}) + \frac{\Delta t}{2} (\mathbf{e}^n + 2\mathbf{e}^{n-1} + \mathbf{e}^{n-2}), \\ \mathbf{F}^{n,**} &= \frac{2\mathbf{a}^{n,*}}{\Delta t} - 2J_0^1 \mathbf{F}^{n-1,*} - 2 \sum_{m=2}^{n-1} J_0^m \mathbf{F}^{n-m} - J_0^n \mathbf{F}^0\end{aligned}\quad (38)$$

followed by the averaging step

$$\mathbf{F}^{n-1} = \frac{1}{4} \mathbf{F}^{n,**} + \frac{1}{2} \mathbf{F}^{n-1,*} + \frac{1}{4} \mathbf{F}^{n-2} \quad (39)$$

and the correction step

$$\begin{aligned}\sigma^n &= \sigma^{n,*} - 2\mathbf{v} \cdot (\mathbf{F}^{n-1} - \mathbf{F}^{n-1,*}), \\ \psi^n &= \psi^{n,*} + \Delta t (\sigma^n - \sigma^{n,*})/2, \\ \mathbf{a}^n &= \mathbf{a}^{n,*} + \frac{\mathbf{v}}{2} (\psi^n - \psi^{n,*}), \\ \mathbf{F}^{n,*} &= \mathbf{F}^{n,**} + \frac{2}{\Delta t} (\mathbf{a}^n - \mathbf{a}^{n,*}) - 2J_0^1 (\mathbf{F}^{n-1} - \mathbf{F}^{n-1,*}).\end{aligned}\quad (40)$$

The whole process above looks quite complicated, but it has been designed for computational efficiency rather than ease of exposition. The main point is that the convolution sums are by far the most expensive part of the calculations, and this arrangement of the time averaging requires that they are computed only once per step. The other calculations add relatively little to the overall time taken by the algorithm. These comments also apply to the fully discretised EFIE schemes, where the dominance of the convolution sum calculation is even greater.

Stability analysis of the scheme defined by Eqs. (38)–(40) is carried out in a similar manner to that in Section 4.1. The algorithm is first condensed by using Eq. (38) to eliminate $\sigma^{n,*}, \psi^{n,*}, \mathbf{a}^{n,*}$ and $\mathbf{F}^{n,**}$ from Eqs. (39) and (40), leaving equations for the five variables $\sigma^n, \psi^n, \mathbf{a}^n, \mathbf{F}^{n,*}$ and \mathbf{F}^{n-1} . The details are tedious, but the system of equations that results has the form

$$\underline{Q}_A^0 \mathbf{z}^n = \mathbf{b}^n + \frac{1}{2} \underline{Q}_A^n \mathbf{z}^0 + \sum_{m=1}^{n-1} \underline{Q}_A^m \mathbf{z}^{n-m},$$

where now \mathbf{z}^n is the vector

$$\mathbf{z}^n = (\sigma^n, \psi^n, \mathbf{a}^n, \mathbf{F}^{n,*}, \mathbf{F}^{n-1})^T \in \mathbb{R}^8,$$

the coefficient matrices are $Q_A^0, Q_A^1, \dots \in \mathbb{R}^{8 \times 8}$ and the inhomogeneous terms are contained in $\mathbf{b}^n \in \mathbb{R}^8$. Following the same process as in Section 4.1, we see that stability of this time-averaged scheme depends on the amplification matrices $P_A^n \in \mathbb{R}^{8 \times 8}$ defined recursively by

$$Q_A^0 P_A^k = \sum_{m=1}^k Q_A^m P_A^{k-m}$$

with $P_A^0 = I_8$, the 8×8 identity matrix. Amplification matrices P_A^n for Schemes 2–4 are derived similarly.

Results of numerical tests to evaluate $\|P_A^n\|_2$ against n are shown in Fig. 4 for Schemes 1 and 4. For Scheme 1, the tests indicate that the limit on the time-step size to avoid exponential instability is cut significantly to about $\nu \leq 1.2$. For the other schemes (including the unconditionally stable trapezoidal rule Scheme 4), the addition of averaging appears to render them exponentially unstable for all but the smallest values of Δt . The exponential growth is quite slow for small Δt , and in these cases it is hard to determine stability or instability with confidence. The behaviour of the staggered grid Scheme 3 is rather unusual since it seems to have a window of stability for $\nu \approx 0.5 \pm 0.1$ and is exponentially unstable otherwise.

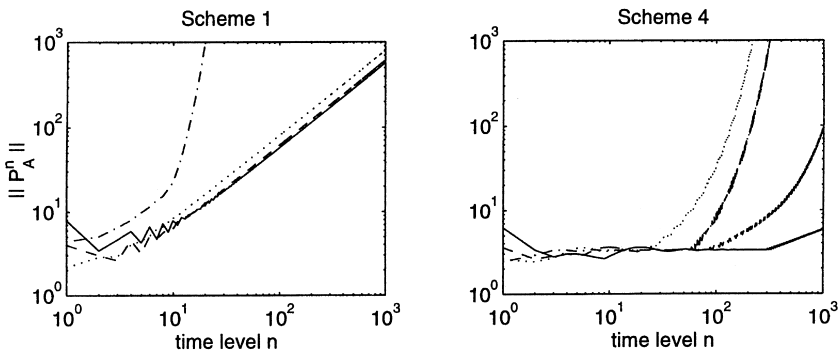


Fig. 4. Graphs of the amplification matrices $\|P_A^n\|_2$ against time level n for the time-averaged versions of Schemes 1 and 4. We have $\nu = \Delta t(1, 2)$ with four different values of Δt such that $\nu = 0.2$ (solid), $\nu = 0.4$ (dashed), $\nu = 0.8$ (dotted) and $\nu = 1.6$ (dash-dot). The stability limit for the un-averaged Scheme 1 is $\nu \leq 2$ and unaveraged Scheme 4 is unconditionally stable.

6. Accuracy

In order to test the performance of the four numerical schemes we need to be able to find the exact solution of the system (6)–(9). The potentials \mathbf{a} and ψ are auxiliary quantities and \mathbf{F} and σ are the variables of physical interest. Unfortunately there are not many choices of the forcing function \mathbf{e} for which exact values of σ and \mathbf{F} can be found explicitly or even just very accurately. The first test we describe below is chosen mainly because it has a straightforward exact solution, while the second is chosen to illustrate what happens with the widely used Gaussian profile incident field.

To see what is required, we consider Eqs. (6), (13) and (12) linking the incident field \mathbf{e} with σ and \mathbf{F} . The equations are repeated here for convenience:

$$\dot{\sigma} + \omega \cdot \mathbf{F} = 0, \quad \dot{\mathbf{F}} - \omega \sigma = \boldsymbol{\varepsilon}, \quad \int_0^t J_0(wR) \boldsymbol{\varepsilon}(t-R) \, dR = \mathbf{e}(t).$$

We generate the first test problem below by choosing $\boldsymbol{\varepsilon}$, calculating \mathbf{e} from the integral and solving the inhomogeneous ODE system for σ and \mathbf{F} . The second is found by choosing \mathbf{F} , calculating σ from the first ODE and $\boldsymbol{\varepsilon}$ from the second, leaving \mathbf{e} to be found from the integral.

In the first test problem we choose $\boldsymbol{\varepsilon} = \omega \boldsymbol{\varepsilon}_0 \sin \omega t$, so that \mathbf{e} can be computed explicitly from the integral (12) (see e.g. Ref. [17], Section 6.674), giving

$$\mathbf{e}(t) = \omega \boldsymbol{\varepsilon}_0 t J_1(\omega t), \quad (41)$$

where J_1 is the first kind Bessel function of order 1. The exact solution for σ is

$$\sigma_e(t) = \alpha(\omega t \cos \omega t - \sin \omega t), \quad (42)$$

where $\alpha = \hat{\mathbf{u}} \cdot \boldsymbol{\varepsilon}_0 / 2$ for $\hat{\mathbf{u}} = \boldsymbol{\omega} / \omega$, and we have used the initial conditions $\sigma(0) = \dot{\sigma}(0) = 0$ (the second equality follows from Eq. (6) because $\mathbf{F} = \mathbf{0}$). Finally, integrating Eq. (13) and using the zero initial conditions gives the exact solution

$$\mathbf{F}_e(t) = \alpha \hat{\mathbf{u}}(\omega t \sin \omega t + 2 \cos \omega t - 2) + \boldsymbol{\varepsilon}_0(1 - \cos \omega t). \quad (43)$$

The solution components σ and \mathbf{F} oscillate with frequency ω and have amplitude growing like $O(t)$. This is illustrated in Fig. 5.

The second test problem has a Gaussian profile pulse-shaped incident field, which is a common test case for scattering problems. To build this test problem, we start with the choice

$$\mathbf{F}(t) = \begin{pmatrix} 1 \\ 1 \end{pmatrix} (t - t_0) e^{-q(t-t_0)^2} \quad (44)$$

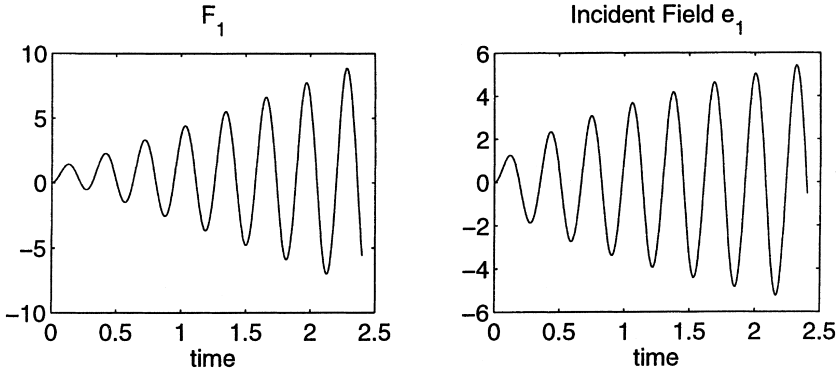


Fig. 5. Incident field and exact solution used in Test 1 given Eqs. (41) and (43) at the relatively high frequency $\omega = (12, 16)$. σ is similar to F_1 but is out of phase with it.

which is concentrated around $t = t_0$, and use the ODE system (13) to obtain

$$\sigma(t) = \left(\frac{\omega_1 + \omega_2}{2q} \right) e^{-q(t-t_0)^2},$$

$$\varepsilon(t) = \begin{pmatrix} 1 - 2q(t - t_0)^2 - \omega_1(\omega_1 + \omega_2)/(2q) \\ 1 - 2q(t - t_0)^2 - \omega_2(\omega_1 + \omega_2)/(2q) \end{pmatrix} e^{-q(t-t_0)^2}.$$

The incident field that generates this solution is then found by substituting the expression for $\varepsilon(t)$ into Eq. (12), and using numerical quadrature to evaluate the incident field $e(t)$ to high accuracy (relative error $\sim 10^{-11}$ or better). Now these functions are not strictly zero for $t \leq 0$, but because they decay so quickly away from $t = t_0$, they can be made insignificantly small when q and t_0 are big enough. We show plots of the components of this solution for the choice $q = 100$, $t_0 = 1$ in Fig. 6.

We show results from both test cases run over the time interval $[0, 2.5]$. The error in F and σ is measured over the whole time interval using the discrete 2-norm, then normalised by dividing by the discrete 2-norm of the exact solution over the same time levels. The schemes are all second order accurate and stable, and so we expect to get second order convergence of the approximations. This is observed in test results shown in Figs. 7 and 8, where all errors behave like $C \Delta t^2$ as $\Delta t \rightarrow 0$. (To verify this, measure the slopes on the log-log plots.) Next we observe that the Scheme 3 results are about four times as accurate as those of Scheme 2 in both tests. This is due to Schemes 2 and 3 using very similar leap-frog approximations of the ODEs, with the effective step size in Scheme 3 being half of the step for Scheme 2. Given the second order accuracy of the

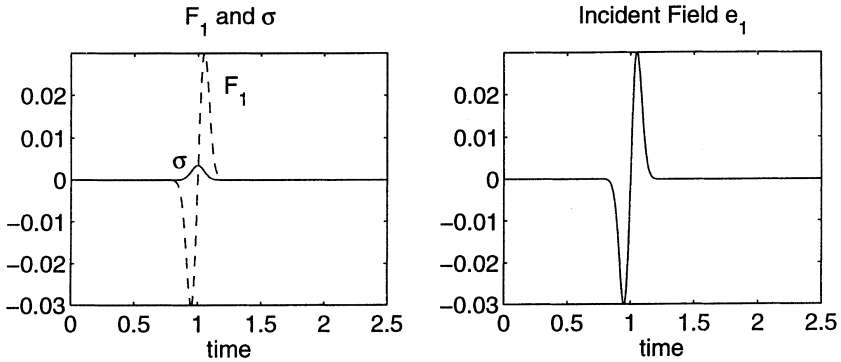


Fig. 6. Incident field and exact solution used in Test 2 determined by Eq. (44) with $q = 100$, $t_0 = 1$ and frequency $\omega = (0.6, 0.8)$. The solution and incident field have a Gaussian profile.

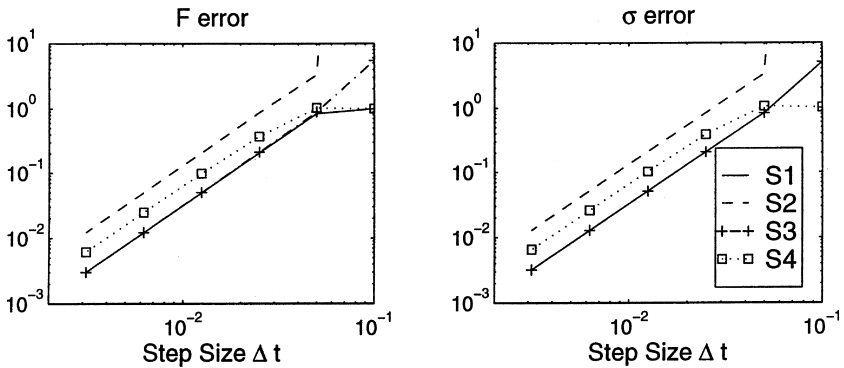


Fig. 7. Test 1 errors in the four schemes for various step sizes Δt with frequency $\omega = (12, 16)$ over time interval $[0, 2.5]$. The results shown are typical of those obtained over a wide range of frequencies.

schemes, this translates to the Scheme 3 results being four times as accurate as those of Scheme 2 as observed.

It is not possible to describe the observed behaviour of Schemes 1 and 4 (Rynne and trapezoidal rule) in such simple terms. An analysis of the local truncation errors of the ODE parts of the schemes suggests that the trapezoidal rule scheme accuracy should lie between that of the two leap-frog schemes, and that is what is seen in test 1. However, this certainly does not hold for the test 2 results, where Scheme 4 is better than both leap-frog schemes. The reason for this is that errors from the RPIE and ODE solutions can interact to give beneficial cancellations for some types of incident field. The Rynne scheme also

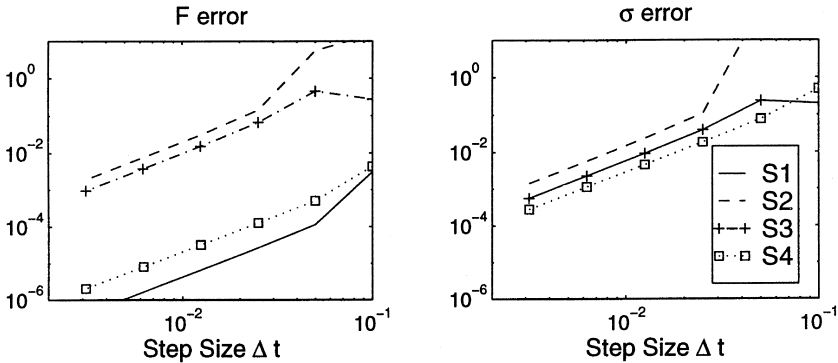


Fig. 8. Test 2 (Gaussian pulse) errors in the four schemes for various step sizes Δt with frequency $\omega = (0.6, 0.8)$ over time interval $[0, 2.5]$. The results shown are typical for frequencies $\omega \leq 1$, but for $\omega > 3$ they look quite similar to the results of test 1.

benefits from these cancellations in test 2, and this is particularly clear for the errors in F .

The main factor behind these error cancellations is the way the incident field e is averaged in the ODE approximations (15) and (22b) for Schemes 1 and 4, respectively. For example, experiments with different combinations of incident field time levels (for example replacing Eq. (15) by Eq. (36)), dramatically reduce the accuracy of Scheme 1 in the test 2 results. To see this, recall that in Section 3.3 we showed that all four schemes implicitly contain approximations of the closed ODE system (6) and (13) for F, σ . The forcing term ε in this ODE system is determined from the incident field e by a trapezoidal rule approximation of the RPIE (12). The averaging used on the incident field e in Schemes 1 and 4 appears in the same form for ε in the approximations (28) and (31) of the ODE for F . It is beneficial because it kills the sawtooth oscillations (see Ref. [14], Ch. 6.10) that appear in trapezoidal rule approximations of first kind Volterra integral equations like (12).

7. Conclusions

We have examined the behaviour of approximations of the full electromagnetic scattering problem (1)–(4) posed on an infinite flat plate, where we treat the space variation exactly and discretise only in time. To do this we first used the classical separation of variables technique (into time and space dependent terms) to obtain the system of ODEs and integral equations (6)–(9) which govern the temporal variation of each spatial mode. (The spatial modes are the usual Fourier modes that appear when separation of variables is

applied to PDEs.) We then examined the behaviour of four different approximation schemes, paying particular attention to stability and accuracy. The first scheme is the space-exact counterpart of the scheme used by Rynne [3] for the full scattering problem, and the others can also be related back to approximations of that problem.

When considering stability of the schemes (without averaging) in Section 4, we found that Scheme 2 (which uses a leap-frog approximation of the ODEs) requires step sizes that are half that required by Schemes 1 and 3 to maintain stability, while Scheme 4 (which uses the trapezoidal rule for the ODEs) is unconditionally stable. Our tests of accuracy in Section 6 show that the errors in all four schemes are $O(\Delta t^2)$ as $\Delta t \rightarrow 0$, but it is hard to generalise about the size of the coefficients of the leading term in the error since these are strongly dependent on the incident field e . We do observe that Scheme 3 is usually 4 times as accurate as Scheme 2, and Schemes 1 and 4 usually perform at least as well as the other two, with Scheme 1 winning in many cases. Also, Schemes 1 and 4 benefit from systematic error cancellation in some problems to give unexpectedly good results.

We have examined the stability of both the unaveraged and averaged versions of the schemes, and the results of Section 5 indicate that the averaged versions of Schemes 2–4 should be rejected because they are exponentially unstable. Note also that the averaged version of Scheme 1 is less stable than its unaveraged version. These results go against the intuition that temporal averaging should make the schemes more stable, and indicate that approximations of the full electromagnetic scattering problem (1)–(4) which have good spatial accuracy are not likely to benefit from being averaged in time.

A summary of results is given in Table 1, and based on the evidence presented for the unaveraged schemes in the table it is clear that Scheme 3 is significantly better than (and hence should always be chosen in preference to) Scheme 2. Scheme 1 seems to be the “best” approximation, since it usually

Table 1
Summary of results from Sections 4 and 6

Scheme	Not averaged		Averaged
	Stable when $\omega\Delta t <$	Size of error (relative to Scheme 3)	Stable when $\omega\Delta t <$
1 (Rynne)	2	0.1–1	1.2
2 (leap-frog)	1	4	Unstable
3 (Staggered leap-frog)	2	1	Unstable
4 (Trapezoidal)	∞	0.5–2	Unstable

The “Size of Error” entry is measured with the same step size Δt and frequency ω . The distinction between “Averaged” and “Not Averaged” refers to the results of Section 5.

gives better results than Schemes 3 and 4, and sometimes gives much better results. However we think that Scheme 4 is worthy of further investigation for the full scattering problem, where its infinite stability interval might help to counteract the instabilities that arise from the complicated interaction between spatial and temporal approximations.

Acknowledgements

P.J. Davies acknowledges the support of the Procurement Executive, DERA.

References

- [1] D.S. Jones, *Methods in Electromagnetic Wave Propagation*, second edition, Clarendon Press, Oxford, 1994.
- [2] B.P. Rynne, P.D. Smith, Stability of time marching algorithms for the electric field equation, *J. Electromag. Waves & Appl.* 4 (1990) 1181–1205.
- [3] B.P. Rynne, Time domain scattering from arbitrary surfaces using the electric field equation, *J. Electromag. Waves & Appl.* 5 (1991) 93–112.
- [4] S.M. Rao, T.K. Sarkar, An alternative version of the time-domain electric field integral equation for arbitrarily shaped conductors, *IEEE Trans. Antennas and Propagation* 41 (1993) 831–834.
- [5] S.M. Rao, D.R. Wilton, Transient scattering by conducting surfaces of arbitrary shape, *IEEE Trans. Antennas and Propagation* 39 (1991) 56–61.
- [6] D.A. Vechinski, S.M. Rao, A stable procedure to calculate the transient scattering by conducting surfaces of arbitrary shape, *IEEE Trans. Antennas and Propagation* 40 (1992) 661–665.
- [7] P.J. Davies, Stability of time-marching numerical schemes for the electric field integral equation, *J. Electromag. Waves & Appl.* 8 (1994) 85–114.
- [8] P.J. Davies, On the stability of time marching schemes for the general surface electric field integral equation, *IEEE Trans. Antennas and Propagation* 44 (1996) 1467–1473.
- [9] P.J. Davies, A stability analysis for the general surface electric field integral equation, *Appl. Numer. Math.* 27 (1998) 33–57.
- [10] P.J. Davies, Numerical stability and convergence of approximations of retarded potential integral equations, *SIAM J. Numer. Anal.* 31 (1994) 856–875.
- [11] P.J. Davies, D.B. Duncan, Averaging techniques for time marching schemes for retarded potential integral equations, *Appl. Numer. Math.* 23 (1997) 291–310.
- [12] B.P. Rynne, Instabilities in time marching methods for scattering problems, *Electromagnetics* 6 (1986) 129–144.
- [13] K.W. Morton, D.F. Mayers, *Numerical Solution of Partial Differential Equations*, Cambridge Univ. Press, Cambridge, 1994.
- [14] C.T.H. Baker, *The Numerical Treatment of Integral Equations*, Clarendon Press, Oxford, 1977.
- [15] R.D. Richtmyer, K.W. Morton, *Difference Methods for Initial-Value Problems*, Wiley, New York, 1967.

- [16] J.D. Lambert, *Numerical Methods for Ordinary Differential Systems*, Wiley, New York, 1991.
- [17] I.S. Gradshteyn, I.M. Ryzhik, *Table of Integrals, Series, and Products*, fifth edition, Academic Press, New York, 1994.